Applied Physics Letters

Atomic layer deposition of TiN/Ru gate in InP MOSFETs

Cite as: Appl. Phys. Lett. **119**, 123502 (2021); https://doi.org/10.1063/5.0058825
Submitted: 02 June 2021 • Accepted: 01 September 2021 • Published Online: 22 September 2021

Hsin-Ying Tseng, Yihao Fang, William James Mitchell, et al.

View Online
Export Citation
CrossMark

ARTICLES YOU MAY BE INTERESTED IN

An 8-nm-thick Sn-doped polycrystalline β-Ga_2O_3 MOSFET with a "normally off" operation
Applied Physics Letters **119**, 122103 (2021); https://doi.org/10.1063/5.0065244

Planar and three-dimensional damage-free etching of β-Ga_2O_3 using atomic gallium flux
Applied Physics Letters **119**, 123503 (2021); https://doi.org/10.1063/5.0057203

P-type $In_xGa_{1-x}N$ semibulk templates ($0.02 < x < 0.16$) with room temperature hole concentration of mid-10^{19} cm^{-3} and device quality surface morphology
Applied Physics Letters **119**, 122101 (2021); https://doi.org/10.1063/5.0065194

QBLOX

Shorten Setup Time
Auto-Calibration
More Qubits

Fully-integrated
Quantum Control Stacks
Ultrastable DC to 18.5 GHz
Synchronized <<1 ns
Ultralow noise

visit our website >

© 2021 Author(s).

Atomic layer deposition of TiN/Ru gate in InP MOSFETs

Cite as: Appl. Phys. Lett. **119**, 123502 (2021); doi: 10.1063/5.0058825
Submitted: 2 June 2021 · Accepted: 1 September 2021 ·
Published Online: 22 September 2021

Hsin-Ying Tseng,[1,a)] Yihao Fang,[1] William James Mitchell,[2] Aidan Arthur Taylor,[3] and Mark J. W. Rodwell[1]

AFFILIATIONS

[1]Department of Electrical and Computer Engineering, University of California Santa Barbara, Santa Barbara, California 93106, USA
[2]UCSB Nanofabrication Facility, University of California Santa Barbara, Santa Barbara, California 93106, USA
[3]Department of Materials Science, University of California Santa Barbara, Santa Barbara, California 93106, USA

[a)]Author to whom correspondence should be addressed: hsinying@ucsb.edu

ABSTRACT

InP channel planar and vertical MOSFETs utilizing atomic layer deposition of a TiN/Ru gate are fabricated. The performance of the TiN/Ru gate is compared to a Ru-only gate based on the C–V characteristics of MOS (metal–oxide–semiconductor) capacitors and peak transconductance (g_m) and subthreshold swing (SS) in planar MOSFETs. Compared to devices with the conventional Ni/Au gate metal, these have a 70 mV/dec SS [Tseng *et al.*, in *Device Research Conference* (IEEE, 2019), pp. 183–184.] and a long gate length; TiN/Ru gate devices exhibit an average 68 mV/dec SS, a record low value of InP, suggesting a high quality, low-damage high-k/InP interface. A record high peak g_m of 0.75 mS/μm at $V_{DS} = 0.6$ V on an InP channel is achieved in a planar gate length (L_g) = 80 nm device. A vertical MOSFET shows a reasonably conformal Ru coverage of the vertical fin and a high 0.42 mS/μm peak g_m for a L_g = 50 nm device. The results of planar and vertical MOSFETs show that TiN/Ru gate metallization via atomic layer deposition is promising for non-planar III–V MOS devices.

Published under an exclusive license by AIP Publishing. https://doi.org/10.1063/5.0058825

III–V Metal–oxide–semiconductor (MOS) structures are of potential interest in III–V MOS high electron mobility transistors (MOSHEMTs),[2,3] targeting applications in mm-wave receivers, and in the gate structure of tunnel FETs for ultra-low voltage VLSI logic.[4–7] MOSFETs with subthreshold swings (SSs) approaching 60 mV/decade have been demonstrated with ZrO_2 and HfO_2 gate dielectrics on InGaAs, InAs, and InP channels, indicating dielectric/semiconductor interface trap densities (D_{it}) less than $3 \times 10^{12}\,cm^{-2}\,eV^{-1}$.[1,8–10] Previous results have generally used gate metals deposited by sputtering or thermal evaporation. For non-planar finFETs and next generation gate-all-around (GAA) nanowire transistors, a more uniform and conformal high-k metal gate (HKMG) is necessary to ensure a low gate resistance and a consistent threshold voltage distribution.[4,11,12] Thus, the atomic layer deposited (ALD) HKMG, with its superior uniformity in thickness and conformity, had been demonstrated in InGaAs FinFETs.[13] There have been no reports of ALD HKMG with low D_{it} on InP channels. Here, we present an ALD low D_{it} Ru/TiN/ZrO_2 HKMG on InP with the lowest *SS* of 68 mV/dec in long gate length planar devices, as well as comparable peak g_m on vertical MOSFETs.

Ruthenium has a desirable metal work function for III–V N-MOSFETs as well as low resistivity and good thermal stability. One key to the successful ALD growth of Ru is controlled nucleation on dissimilar materials.[14] Nucleation and growth initiation of ALD Ru appear to vary with substrates used. Rough and non-uniform growth on SiO_2, low-k dielectrics, and TaN surfaces has been reported.[15–17] Films with poor nucleation have also exhibited poor electrical properties.[18] Yim *et al.* reported ALD Ru with an improved nucleation on a thin SiN_x or heavily NH_3-plasma activated (50 min exposure) SiO_2 surface according to TEM analysis.[16] Zhang *et al.*, on the other hand, demonstrated improved ALD Ru nucleation with an Al_2O_3 surface layer.[19] Overall, it was suggested that one can improve the nucleation of Ru growth by surface energy engineering, which helps with the adsorption of Ru precursors.[20] The addition of an Al_2O_3 interlayer and plasma treatment prior to Ru deposition in MOS structures, however, may degrade device electrical performance due to increased effective-oxide-thickness (EOT), increased interface trap density, and a shift in the MOS threshold voltage. Therefore, it is important to consider trade-offs in ALD Ru HKMG design between Ru film quality and overall device performance. In this work, a thin ALD TiN layer (~2 nm) is deposited as a nucleation/stiction layer in Ru gate devices.[21] TiN/Ru gates and Ru-only gates on the InP channel are compared. The capacitance–voltage (C–V) characteristics of metal–oxide–semiconductor capacitors (MOSCAPs) structures, and SS and peak g_m of planar MOSFETs, are employed to evaluate the

Published under an exclusive license by AIP Publishing

performance of the two metal gate stacks. Ru growth is further optimized for a better conformity. At last, vertical MOSFETs with conformal TiN/Ru gates are demonstrated. Transfer and output characteristics of vertical MOSFETs are compared to their planar counterpart.

Planar MOSFETs were fabricated on semi-insulating (SI) (100) Fe-doped InP substrates. The fabrication started with epitaxial growth of the channel by metal organic chemical vapor deposition (MOCVD). The MOCVD channel growth was performed at 600 °C and consists of a bottom 9 nm, 8×10^{17} cm^{-3} Zn-doped *P*-InP layer to compensate for the donor impurities at the growth interface, and a top 9 nm unintentionally doped (UID) InP layer. After the channel growth, a dummy gate was defined by electron beam lithography (EBL) using hydrogen silsesquioxane (HSQ) resist for subsequent self-aligned raised source/drain MOCVD regrowth. A 1-min dip in HCl:H_2O 1:10 was done prior to the regrowth. For the source/drain, a 9 nm UID InP spacer, a 10 nm, 2×10^{19} cm^{-3} Si-doped N^+-InP, and 110 nm, 4×10^{19} cm^{-3} Si-doped N^+-$In_{0.53}Ga_{0.47}As$ layers were grown at 600 °C. Devices were then isolated by selective wet etch using HCl- and H_3PO_4:H_2O_2-based solutions. After a 2-min buffered HF (BHF) dip followed by one cycle of a HCl-based digital etch to remove the dummy gate and surface oxides, high-k and metal gate layers were deposited in an Oxford FlexAL ALD system. The high-k deposition process includes initial surface passivation using nine cycles of alternating N_2-plasma and trimethylaluminum (TMAl) dosing (~1 nm AlO_xN_y)[9,22] followed by 40 cycles of H_2O and tetrakis(ethylmethylamido)zirconium (TEMAZ) dosing (~2.5 nm ZrO_2) at 300 °C.[23] To further passivate surface dangling bonds, a 30-min ALD *in situ* H_2 anneal was performed at 350 °C. Metal gate deposition at 300 °C utilizes a 35-cycle TiN nucleation layer (~2 nm) first deposited using tetrakis(dimethylamido)titanium (TDMAT) together with a N_2- and H_2-plasma [400 W inductively coupled plasma (ICP) power]. Five hundred cycles of ALD Ru (~30 nm) was then deposited using (ethylbenzene)(1,3-cyclohexadiene)ruthenium (EBCHDRu) and O_2 cycles at 300 °C. EBCHDRu is a zero-valent organometallic precursor (Hansol Chemical, Korea). *In situ* post-metal annealing in H_2 ambient at 350 °C was employed for 30 min to recover plasma damage at the high-k/InP interface. Ru metal gate patterns were dry etched using an O_2-based ICP etch (catalyzed with a small of amount of Cl_2).[24] The TiN and the high-k dielectric layers were etched via a 1-min BHF dip. Source and drain metal contacts (Ti/Pd/Au) were deposited by lift-off. Devices were finally passivated using Al_2O_3 (~3 nm) deposited by ALD.

The vertical MOSFETs were fabricated in a top-down process. The epitaxial stack consisted of, from bottom to top, a Fe-doped SI (100) InP substrate, a 90 nm thick Si-doped N^+-$In_{0.53}Ga_{0.47}As$ (4×10^{19} cm^{-3}) source layer, 5 nm thick Si-doped N^+-InP (2×10^{19} cm^{-3}) layer, a 50 nm thick Zn-doped P-InP (1×10^{18} cm^{-3}) channel layer, a 5 nm thick Si-doped N^+-InP (2×10^{19} cm^{-3}) drain layer, and a 10 nm thick Si-doped N^+-$In_{0.53}Ga_{0.47}As$ (4×10^{19} cm^{-3}) contact layer. All layers were grown by MOCVD at 600 °C. A refractory Mo/TiW (20/500 nm) drain metal contact was deposited by electron beam deposition and DC sputtering, respectively, and then patterned using EBL followed by ICP etching.[25] A 20 nm SiN_x sidewall was formed by plasma-enhanced chemical vapor deposition (PECVD) followed by an anisotropic CF_4-based plasma etch. The 10 nm InGaAs contact layer was wet etched in H_3PO_4: H_2O_2: H_2O 1:1:25. A second 20 nm Si_3N_4 sidewall was then formed. The InP drain and channel were wet etched in HCl:H_3PO_4 1:4. The vertical surface sidewalls of the p-type InP layer acted as the transistor channel. Prior to high-k deposition, five cycles of HCl-based digital etching were performed for native oxide removal on the channel surface. The high-k deposition, H_2 annealing, and TiN deposition processes were identical to the fabrication of the planar MOSFET's detailed above. The ALD Ru deposition, on the other hand, had to be carried out at a lower temperature of 250 °C to ensure conformal growth on the sidewalls of the vertical MOSFET structure (avoiding a small precursor decomposition on the structure at 300 °C).[26,27] To avoid formation of surface RuO_2 during this lower temperature Ru process, a layer that inhibits the growth of a metallic Ru layer, H_2 is added as a reducing co-reactant in the ALD growth cycle.[28] The same post-metal annealing and TiN/Ru patterning steps for planar MOSFETs were employed. The Ti/Pd/Au source contact metal was evaporated and lifted off. Ti/Au metal posts were deposited on the source and gate contacts for back-end wiring. A 30 nm PECVD SiN_x passivation layer was deposited prior to planarization with spin-on dielectric benzocyclobutene (BCB). The BCB dielectric was baked at 250 °C for 1 h and ashed back with a ICP CF_4/O_2 plasma. The SiN_x passivation layer was removed in a BHF dip to expose the TiW drain contact. Excess Ru/TiN/high-k stack that surrounded the TiW/Mo drain contact was wet etched using ruthenium etchant (Transcene RU-44) and BHF. A thick 60 nm SiN_x sidewall spacer was formed by PECVD followed by CF_4-based plasma etch to prevent drain-to-gate short. Finally, Ti/Au (15/10000 nm) metal pads were lifted off to finish the back-end wiring.

Non-uniform substrate color after Ru deposition on ZrO_2 was sometimes observed, suggesting a less than ideal Ru nucleation on ZrO_2. By depositing a thin TiN layer (via ALD) prior to Ru growth, uniform nucleation on any arbitrary substrate is realized. Figure 1 shows the C–V characteristics of InP MOSCAPs with (a) TiN/Ru and (b) Ru gates measured from 1 kHz to 1 MHz. The threshold voltage of TiN/Ru gate MOSCAP is 0.25 V, which is lower than the 0.4 V measured for the Ru-only gate. The large apparent increase in capacitance in accumulation at low frequencies f is a measurement artifact due to gate leakage, as the conductivity dI/dV becomes comparable to $2\pi fC$, where C is the capacitance. The leakage current of the MOSCAPs is ~30 mA/cm^2 at $V_g = 1$ V and is similar for both Ru and TiN/Ru gates. A larger frequency dispersion for Ru gate MOSCAP in depletion can be seen. In comparison, the TiN/Ru gate MOSCAP shows smaller frequency dispersion, suggesting a metal–semiconductor interface with low defect density. Furthermore, the C–V characteristic of the TiN/Ru gate MOSCAP is comparable with that using a thermally evaporated Ni/Au gate, which confirms a high quality high-k/InP interface and a low-damage gate metallization process.[1] This suggests that adding a thin TiN layer not only improves the nucleation of Ru but also resolves the frequency dispersion in the case of Ru-only gates.

Figure 2 shows the schematic planar MOSFET structure used in this study (a) and the TEM images of a $L_g = 30$ nm MOSFET (b). The recess structure and UID InP spacer are used to suppress band-to-band tunneling (BTBT) arising at the high-field region near the drain end of the channel.[29] The regrowth facet with HSQ mask shows a ~30° incline at the channel after InP growth and a ~54° incline after InGaAs growth. The corresponding InP spacer thickness at the channel is approximately 5 nm. The inner highlight in Fig. 2(b) is high-angle annular dark-field imaging (HAADF) STEM image. The

Published under an exclusive license by AIP Publishing

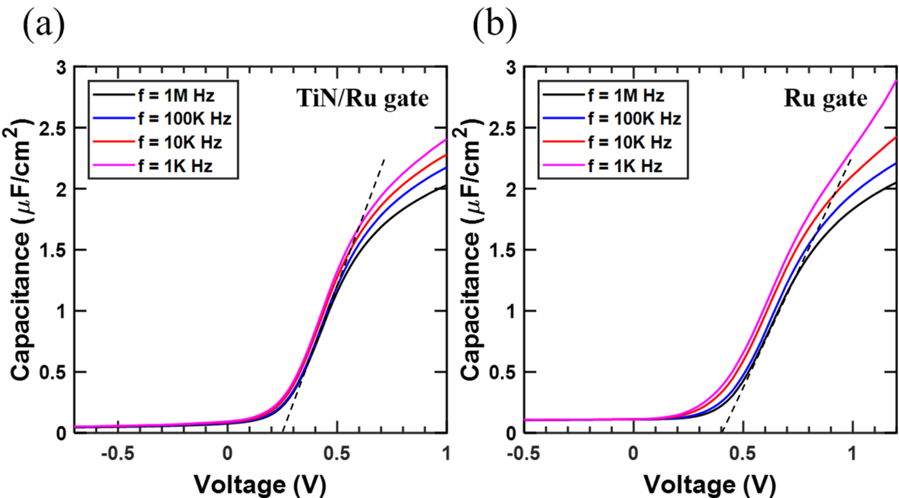

FIG. 1. The C–V characteristic of InP channel MOSCAPs with (a) the TiN/Ru gate and (b) the Ru gate. The large increase in capacitance in accumulation region at low frequencies is a measurement artifact due to gate leakage, arising when G/ω becomes comparable to the capacitance. The TiN/Ru gate shows much less frequency dispersion in the depletion region, indicating a high quality high-k/InP interface and low damage gate metallization.

interfacial layers contain ~1/2.5/2 nm AlO_xN_y/ZrO_2/TiN, as indicated by layers 1, 2, and 3, respectively. In addition, the thickness of Ru film in the channel is ~10 nm, which is much thinner than thickness in-field (~25 nm). This variability in thickness does not affect the DC performances of the planar MOSFETs, but could potentially increase the gate resistance or even result in gate open-circuits in more complex vertical transistor structures that require the gate metal to contacting the sidewall channel. Therefore, a more conformal Ru deposition is needed for vertical MOSFETs and a process to improve Ru conformity will be discussed later.

The gate length of fabricated planar MOSFETs ranges from 30 nm to 2 μm. The transfer and output characteristics of TiN/Ru gate planar MOSFETs with L_g = 30, 80, 200 nm are shown in Fig. 3. The regrown N^+ S/D layer sheet resistance is ~14 Ω, while the S/D contact resistivity is 7 $\Omega\,\mu m^2$, as determined by the transmission line method (TLM). At $L_g > 200$ nm, a more than five orders of magnitude on/off ratio is achieved. The peak g_m of ~0.75 mS/μm is for a L_g = 80 nm MOSFET at V_{DS} = 0.6 V. This is the highest peak g_m reported for InP channel MOSFETs. Due to a comparably thick channel of ~18 nm, MOSFETs with $L_g < 80$ nm suffer short-channel effects. At L_g = 30 nm, the on/off ratio drops to the order of 1000:1, and the peak g_m decreases. In addition, all the planar MOSFETs here reported have significant gate leakage ($|I_G|$) of ~10^{-4} mA per μm of gate width, as can been seen in transfer curves. The high $|I_G|$ arises from parasitic TiN/Ru present on the sidewalls of the N^+ S/D mesa. Given the large perimeter of the transistor mesa, the estimated parasitic area so covered is ~100:1 greater than the device active gate region. The gate leakage per total MOS junction area, gate and sidewall, in the planar MOSFETs is similar to that observed in the MOSCAPs.

Figure 4 summarizes (a) peak g_m vs L_g at V_{DS} = 0.6 V and (b) SS vs L_g with ALD Ru gates, TiN/Ru gates (this work), and thermal evaporated Ni/Au gate MOSFETs.[1] Note that the channel thickness in this work is ~18 nm, which is ~4 nm thicker than for the Ni/Au gate MOSFETs plotted in Fig. 4. Transistors with ALD TiN/Ru gates had the highest peak g_m of ~0.75 mS/μm for a L_g = 80 nm transistor. In comparison, Ru-only gates show lower peak g_m, which is consistent with the larger observed frequency dispersion in C–V characteristics as shown before. In addition, the Ru-only gate MOSFETs showed wide variations in characteristics between devices and low yield due to poor nucleation of Ru on the high-k gate dielectric. Correlating with the observed C–V dispersion of MOSCAPs using Ru-only gates, the *SS* of MOSFETs using Ru-only gates is >80 mV/dec even at long gate lengths.

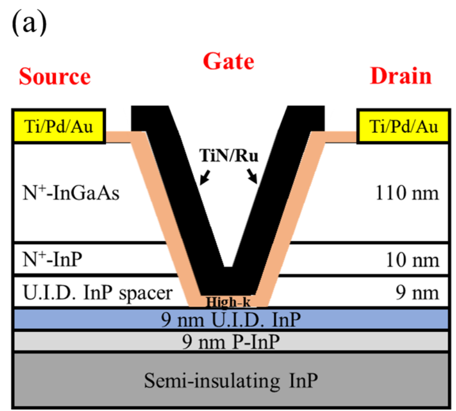

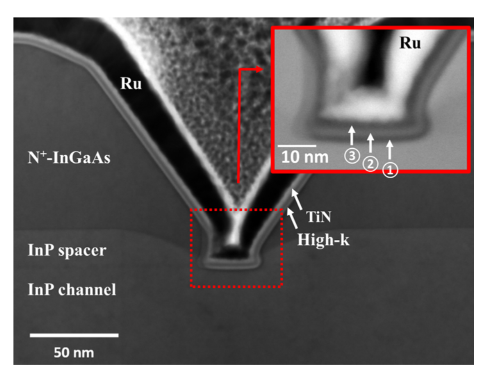

FIG. 2. (a) The cross-sectional planar MOSFET structure and (b) the STEM image of a L_g = 30 nm MOSFET with the TiN/Ru gate. The inner plot in (b) is the HAADF-STEM image highlighting the structure at the InP channel. Layers 1, 2, and 3 represent ~1 nm AlO_xN_y, ~2.5 nm ZrO_2, and ~2 nm TiN, respectively.

Published under an exclusive license by AIP Publishing

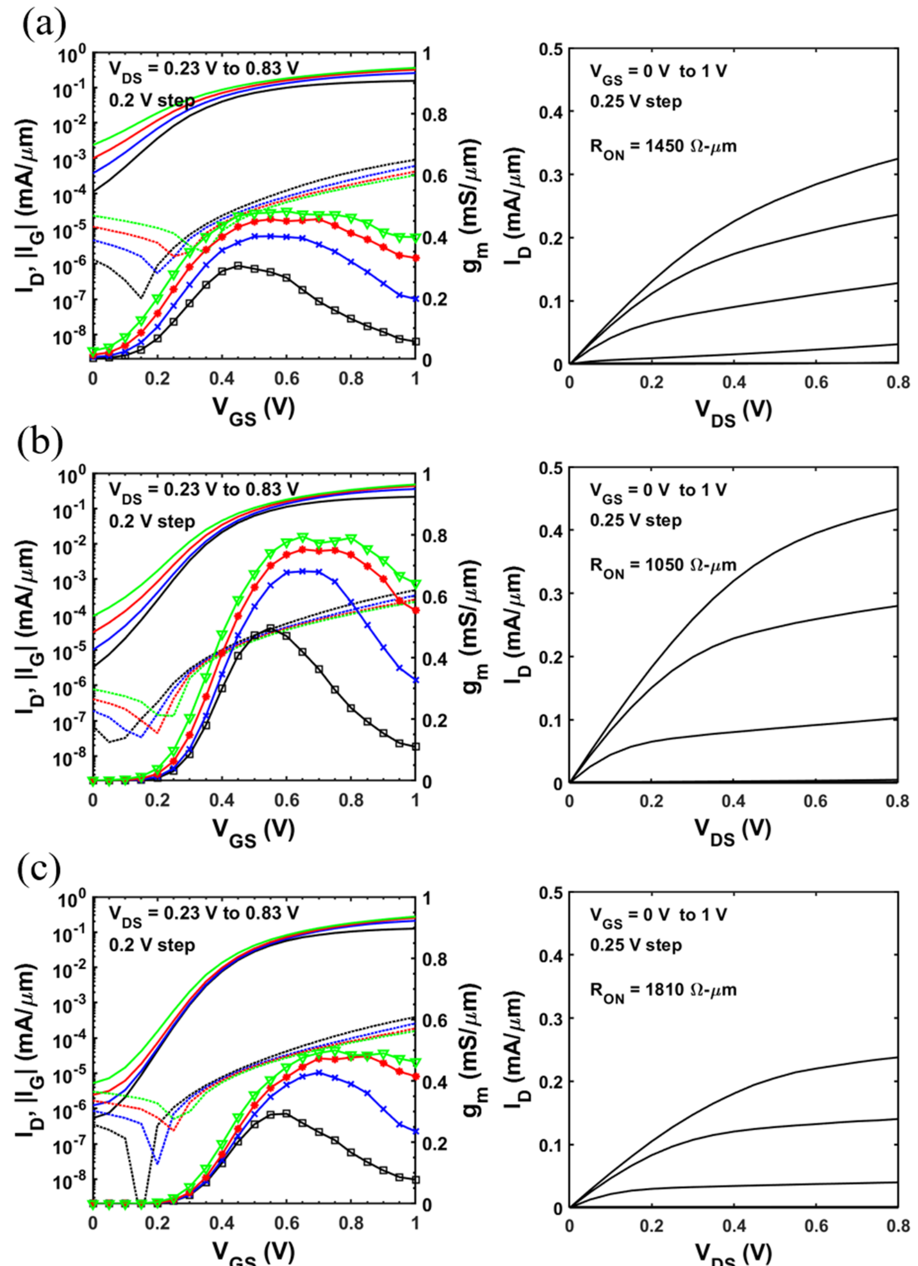

FIG. 3. Transfer (left) and output (right) characteristics of TiN/Ru gates planar MOSFETs with L_g = 30 nm (a), 80 nm (b), and 200 nm (c). In transfer characteristics, solid lines, dotted lines, and symbolic lines represent I_D, $|I_G|$, and g_m, respectively.

A record low SS, for an InP channel, of 68 mV/dec at V_{DS} = 0.1 V for TiN/Ru gate MOSFETs is measured over ten different >800 nm-L_g devices. This value is lower than the previously reported 70 mV/dec on thermal Ni/Au MOSFETs.[1] From this, we calculate the D_{it} of $\sim 1 \times 10^{12}\,\mathrm{cm^{-2}\,eV^{-1}}$, consistent with MOSCAP test structure results. Compared to the thermal Ni/Au gate, the ALD TiN/Ru gate exhibits a lower MOSCAP frequency dispersion under depletion, indicative of lower D_{it} near to band edge. This is consistent with the superior g_m and SS observed with MOSFETs using the ALD TiN/Ru gate.

As pointed out earlier, although ALD growth of Ru at 300 °C yields a high conductivity metallic film, it is compromised by inadequate conformality on sidewalls due to a small amount of thermal decomposition of the precursor.[26,27] For improved step/sidewall coverage, an essential requirement for non-planar structures, deposition at 250 °C, is employed on vertical MOSFETs instead. Figures 5(a) and 5(b) show the cross sectional and top-view of a vertical MOSFET structure. The TEM image, as shown in Fig. 5(c), is the cross-sectional cut along A and A′ as indicated in Fig. 5(b). The image shows that the InP channel is covered by a uniform TiN/Ru film. The 250 °C Ru film

Published under an exclusive license by AIP Publishing

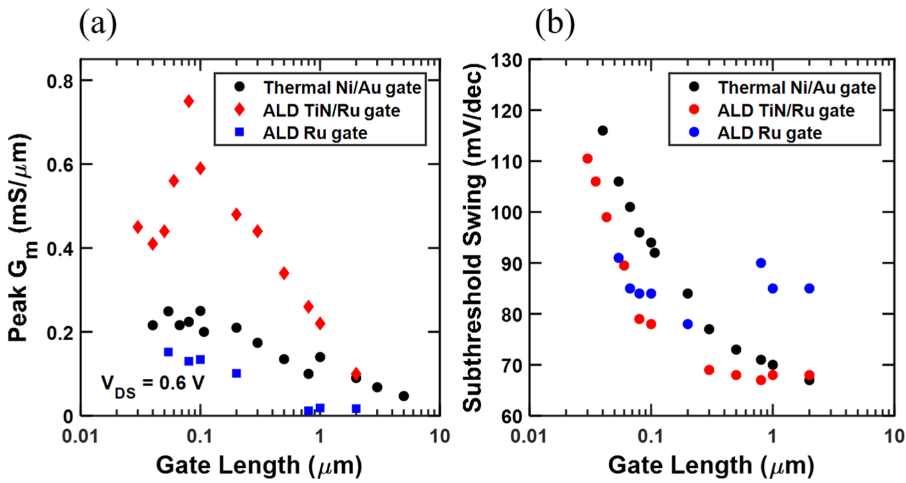

FIG. 4. The comparison of peak g_m vs L_g (a) and the minimum SS vs L_g (b) for InP planar MOSFETs with thermal evaporated Ni/Au gates,[1] ALD TiN/Ru gates, and ALD Ru gates. The average minimum SS for ten MOSFETs (L_g >800 nm) with TiN/Ru gates is 68 mv/dec, which is the record low SS for InP channel MOSFETs. Reproduced with permission from Tseng *et al.*, in *Device Research Conference* (IEEE, 2019), pp. 183–184. Copyright 2019 IEEE.

shows conformally underfilling of notches near to the InP channel and almost constant thickness on the sidewalls and in the field, on top of the N^+ InGaAs source. The TEM image shows an air gap between the BCB planarization material and the Ti/Au pad metal; this may be due to BCB contraction during the relatively high temperature Ti/Au deposition.[30]

The I_D–V_D and I_D–V_G characteristics of vertical MOSFETs with TiN/Ru gate are shown in Figs. 6(a) and 6(b). As can be seen, strong short-channel characteristics are observed. The low aspect ratio between gate length and fin width (50:90 nm) results in poor gate electrostatics. Despite the higher bulk potential barrier in the P-InP channel with a doping concentration of $1 \times 10^{18}\,cm^{-3}$, high leakage current density in the thick InP is present. To overcome this issue, a higher P channel doping or a higher aspect ratio between L_g and body thickness (t_{body}) is needed. Nevertheless, peak g_m at $V_{DS} = 0.6$ V of the vertical MOSFETs measures 0.42 mS/μm, comparable with the

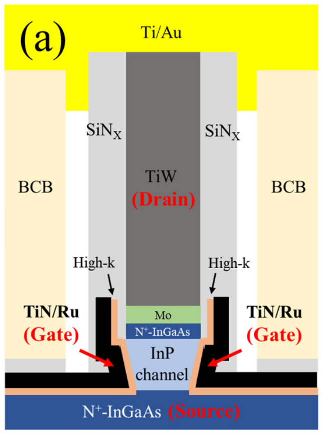

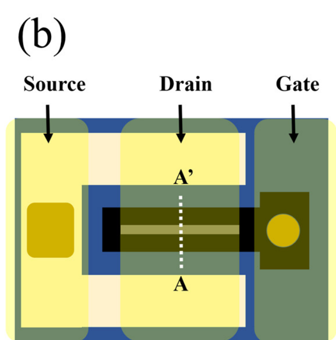

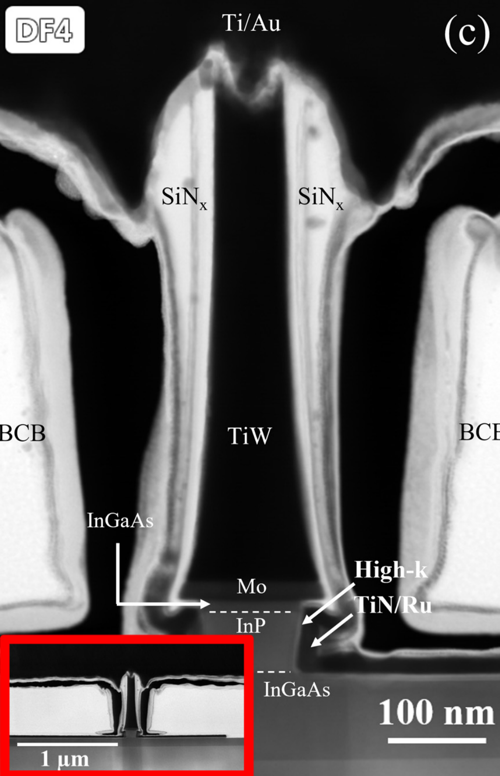

FIG. 5. The schematic (a) cross-sectional and (b) top view vertical MOSFET structure, and (c) the cross-sectional STEM image of the vertical MOSFET with TiN/Ru gate cutting along A and A′, as indicated in (b). The P-InP channel length is 50 nm in this study, while the TiW/Mo drain metal stack is as thick as ∼520 nm to facilitate contacting the drain. The inner plot in (c) is the image in a large field.

Published under an exclusive license by AIP Publishing

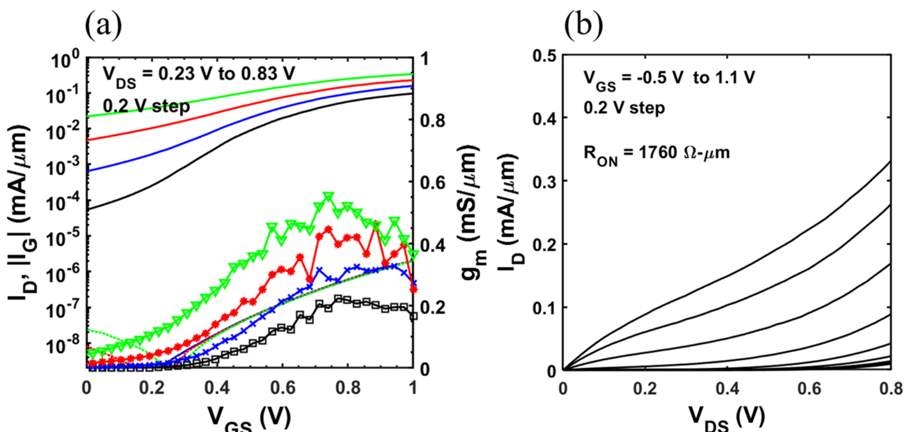

FIG. 6. The transfer (a) and output (b) characteristics for vertical MOSFETs with TiN/Ru gate. In transfer characteristic, solid lines, dotted lines, and symbolic lines represent I_D, $|I_G|$, and g_m, respectively. Low ratio between gate length and fin width (50 nm: 90 nm) results in a poor gate control and shows a strong short channel behavior. The peak g_m at V_{DS} = 0.6 V is ∼0.42 mS/μm, which is closed to planar MOSFET with L_g = 50 nm as shown in Fig. 4(a).

L_g = 50 nm TiN/Ru gate planar MOSFET. This confirms ALD TiN/Ru/high-k gate's low surface trap density on non-planar InP device structures.

In summary, planar and vertical InP channel MOSFETs using an ALD TiN/Ru gate are fabricated. The TiN/Ru gate exhibits better performance than Ru-only gates in MOSCAP C–V characteristics, and in the SS and g_m in planar MOSFETs. The TiN/Ru gate also shows less frequency dispersion along with a record low average SS of 68 mV/dec in long gate length devices, indicating a high quality ZrO_2/InP interface and a low-damage gate metallization process. By utilizing TiN/Ru gates in scaled planar MOSFETs, a record high ∼0.75 mS/μm peak g_m for InP is observed at L_g = 80 nm and V_{DS} = 0.6 V. Vertical MOSFET utilizing TiN/Ru gates is also demonstrated. The vertical transistor shows a similar ∼0.42 mS/μm peak g_m at V_{DS} = 0.6 V at the same 80 nm gate length as the planar MOSFET, which confirms the applicability of this gate metallization process in non-planar structures.

This research was funded by the National Science Foundation (NSF) (Grant No. 1640030) and by the Semiconductor Research Corporation (Grant No. 2016-EP-2694-A), and made use of shared facilities of the UCSB MRSEC (No. NSF DMR 1720256) and the UCSB Nanofabrication facility, an open access laboratory. This work utilized in part the UCSB HFM Lab with instrumentation supported by ONR (Dr. P. Maki) and ARO (Dr. J. Harvey) DURIP grants.

DATA AVAILABILITY

The data that support the findings of this study are available from the corresponding author upon reasonable request.

REFERENCES

[1]H. Y. Tseng, Y. Fang, S. Zhong, and M. J. W. Rodwell, in *Device Research Conference* (IEEE, 2019), pp. 183–184.
[2]A. Tessmann, A. Leuther, F. Heinz, F. Bernhardt, L. John, H. Massler, L. Czornomaz, and T. Merkle, IEEE J. Solid-State Circuits **54**, 2411 (2019).
[3]B. Markman, S. T. S. Brunelli, A. Goswami, M. Guidry, and M. J. W. Rodwell, J. Electron Devices Soc. **8**, 930 (2020).
[4]E. Memisevic, J. Svensson, M. Hellenbrand, E. Lind, and L. E. Wernersson, in *Technical Digest-International Electron Devices Meeting (IEDM)* (IEEE, 2017), pp. 19.1.1–19.1.4.
[5]C. Convertino, K. E. Moselund, C. B. Zota, Y. Baumgartner, P. Staudinger, M. Sousa, S. Mauthe, D. Caimi, L. Czornomaz, and A. M. Ionescu, in *Technical Digest-International Electron Devices Meeting (IEDM)* (IEEE, 2019), pp. 2019–2022.
[6]A. Alian, S. E. Kazzi, A. Verhulst, A. Milenin, N. Pinna, T. Ivanov, D. Lin, D. Mocuta, and N. Collaert, in Digest Technical Paper-Symposium on VLSI Technology (2018), pp. 133–134.
[7]C. Y. Chen, H. Y. Tseng, H. Ilatikhameneh, T. A. Ameen, G. Klimeck, M. J. Rodwell, and M. Povolotskyi, IEEE Trans. Electron Devices **68**, 3104 (2021).
[8]S. Lee, V. Chobpattana, C.-Y. Huang, B. J. Thibeault, W. Mitchell, S. Stemmer, A. C. Gossard, and M. J. W. Rodwell, in *Digest Technical Paper-Symposium on VLSI Technology* (IEEE, 2014), pp. 1–2.
[9]V. Chobpattana, E. M. Mates, J. Y. Zhang, and S. Stemmer, Appl. Phys. Lett. **104**, 182912 (2014).
[10]O.-P. Kilpi, J. Wu, J. Svensson, E. Lind, and L.-E. Wernersson, in *Digest Technical Paper-Symposium on VLSI Technology* (IEEE, 2017), pp. 36–37.
[11]D. Hisamoto, W. Lee, J. Kedzierski, H. Takeuchi, K. Asano, C. Kuo, E. Anderson, T. King, J. Bokor, and C. Hu, IEEE Trans. Electron Devices **47**, 2320 (2000).
[12]K. H. Yeo, S. D. Suk, M. Li, Y. Y. Yeoh, K. H. Cho, K. H. Hong, S. K. Yun, M. S. Lee, N. Cho, K. Lee, D. Hwang, B. Park, D. W. Kim, D. Park, and B. Il Ryu, in *Technical Digest-International Electron Devices Meeting (IEDM)* (IEEE, 2006).
[13]J. J. Gu, X. W. Wang, H. Wu, J. Shao, A. T. Neal, M. J. Manfra, R. G. Gordon, and P. D. Ye, in *Technical Digest-International Electron Devices Meeting (IEDM)* (IEEE, 2012), pp. 633–636.
[14]S. N. Chopra, M. F. J. Vos, M. A. Verheijen, J. G. Ekerdt, W. M. M. Kessels, and A. J. M. Mackus, J. Vac. Sci. Technol. A **38**, 062402 (2020).
[15]M. Zhou, T. Chen, J. J. Tan, G. P. Ru, Y. L. Jiang, R. Liu, and X. P. Qu, Chin. Phys. Lett. **24**, 1400 (2007).
[16]S. S. Yim, D. J. Lee, K. S. Kim, S. H. Kim, T. S. Yoon, and K. B. Kim, J. Appl. Phys. **103**, 113509 (2008).
[17]J. Heo, S. Y. Lee, D. Eom, C. S. Hwang, and H. J. Kim, Electrochem. Solid-State Lett. **11**, G5 (2008).
[18]R. J. Martín-Palma and C. G. Pantano, Mater. Res. Express **6**, 086457 (2019).
[19]M. Zhang, W. Chen, S.-J. Ding, X.-P. Wang, D. W. Zhang, and L.-K. Wang, J. Vac. Sci. Technol. A **25**, 775 (2007).
[20]J. Soethoudt, F. Grillo, E. A. Marques, J. R. van Ommen, Y. Tomczak, L. Nyns, S. Van Elshocht, and A. Delabie, Adv. Mater. Interfaces **5**, 1800870 (2018).
[21]L. G. Wen, P. Roussel, O. V. Pedreira, B. Briggs, B. Groven, S. Dutta, M. I. Popovici, N. Heylen, I. Ciofi, K. Vanstreels, F. W. Østerberg, O. Hansen, D. H. Petersen, K. Opsomer, C. Detavernie, C. J. Wilson, S. Van Elshocht, K. Croes, J. Bömmels, Z. Tőkei, and C. Adelmann, ACS Appl. Mater. Interfaces **8**, 26119 (2016).
[22]V. Chobpattana, T. E. Mates, W. J. Mitchell, J. Y. Zhang, and S. Stemmer, J. Appl. Phys. **114**, 154108 (2013).
[23]J. Wu, Y. Fang, B. Markman, H. Tseng, and M. J. W. Rodwell, IEEE Electron Device Lett. **39**, 472 (2018).
[24]W. J. Mitchell, B. J. Thibeault, D. D. John, and T. E. Reynolds, J. Vac. Sci. Technol. A **39**, 043204 (2021).

Published under an exclusive license by AIP Publishing

[25]Y. Fang, H. Tseng, and M. J. W. Rodwell, in *Device Research Conference* (IEEE, 2019), pp. 179–180.
[26]S. Cwik, K. N. Woods, M. J. Saly, T. J. Knisley, and C. H. Winter, J. Vac. Sci. Technol. A **38**, 012402 (2020).
[27]S. Yeo, S. H. Choi, J. Y. Park, S. H. Kim, T. Cheon, B. Y. Lim, and S. Kim, Thin Solid Films **546**, 2 (2013).
[28]J. Lu and J. W. Elam, Chem. Mater. **27**, 4950 (2015).
[29]C. Y. Huang, S. Lee, V. Chobpattana, S. Stemmer, A. C. Gossard, B. Thibeault, W. Mitchell, and M. Rodwell, in *Technical Digest-International Electron Devices Meeting (IEDM)* (IEEE, 2015), pp. 25.4.1–25.4.4.
[30]S. Seok, IEEE Trans. Compon., Packag., Manuf. Technol. **6**, 1301 (2016).

Published under an exclusive license by AIP Publishing